PNAS RESEARCH ARTICLE | GENETICS OPEN ACCESS

The mismatch recognition protein MutSα promotes nascent strand degradation at stalled replication forks

Junqiu Zhang[a], Xin Zhao[a], Lu Liu[a], Hao-Dong Li[b], Liya Gu[a], Diego H. Castrillon[b], and Guo-Min Li[a,1]

Edited by Wei Yang, National Institutes of Health, Bethesda, MD; received February 1, 2022; accepted September 3, 2022

Mismatch repair (MMR) is a replication-coupled DNA repair mechanism and plays multiple roles at the replication fork. The well-established MMR functions include correcting misincorporated nucleotides that have escaped the proofreading activity of DNA polymerases, recognizing nonmismatched DNA adducts, and triggering a DNA damage response. In an attempt to determine whether MMR regulates replication progression in cells expressing an ultramutable DNA polymerase ε (Polε), carrying a proline-to-arginine substitution at amino acid 286 (Polε-P286R), we identified an unusual MMR function in response to hydroxyurea (HU)-induced replication stress. Polε-P286R cells treated with hydroxyurea exhibit increased MRE11-catalyzed nascent strand degradation. This degradation by MRE11 depends on the mismatch recognition protein MutSα and its binding to stalled replication forks. Increased MutSα binding at replication forks is also associated with decreased loading of replication fork protection factors FANCD2 and BRCA1, suggesting blockage of these fork protection factors from loading to replication forks by MutSα. We find that the MutSα-dependent MRE11-catalyzed fork degradation induces DNA breaks and various chromosome abnormalities. Therefore, unlike the well-known MMR functions of ensuring replication fidelity, the newly identified MMR activity of promoting genome instability may also play a role in cancer avoidance by eliminating rogue cells.

replication fork stability | MutSα | nascent strand degradation | chromosome instability

Significance

DNA mismatch repair (MMR) is well known for its role in maintaining replication fidelity by correcting mispairs generated during replication. Here, we identify an unusual MMR function to promote genome instability in the replication stress response. Under replication stress, binding of the mismatch recognition protein MutSα to replication forks blocks the loading of fork protection factors FANCD2 and BRCA1 to replication forks and promotes the recruitment of exonuclease MRE11 onto DNA to nascent strand degradation. This MutSα-dependent MRE11-catalyzed DNA degradation causes DNA breaks and chromosome abnormalities, contributing to an ultramutator phenotype.

Accurate DNA replication is essential for genome integrity. In mammalian cells, faithful replication relies on the DNA mismatch repair (MMR) pathway and the proofreading activity of DNA polymerases ε (Polε) and δ (Polδ) (1–4), which are responsible for synthesizing the leading and lagging strands, respectively (1, 5). While Polε and Polδ use their 3′ to 5′ exonuclease activity to directly remove misincorporated nucleotides, MMR corrects biosynthetic errors that have escaped the proofreading activity of Polε and Polδ. The importance of MMR in genome maintenance is underscored by the fact that defects in MMR lead to hereditary and sporadic colorectal cancers, as well as other malignancies (2, 4, 6–8).

Human MMR has been reconstituted using purified proteins, including MutSα (MSH2-MSH6), MutLα (MLH1-PMS2), PCNA (proliferating cell nuclear antigen), RPA (replication protein A), exonuclease 1 (Exo1), RFC (replication factor C), and Polδ (9, 10). Interestingly, many of these proteins such as PCNA, RPA, RFC, and Polδ, also participate in DNA replication, consistent with the notion that MMR is coupled to replication (11, 12). In bacteria, the methyl-directed MMR has a window of 3 to 4 min to repair misincorprated bases, as newly synthesized unmethylated d(GATC) sequences, which serve as the strand discrimination signal for MMR, are fully methylated within 5 min after synthesis (13). Similarly, newly synthesized DNA in eukaryotic cells is immediately packed into nucleosomes (14). Thus, the MMR system and replication machinery must be coordinated in a manner allowing misincorporated bases to be removed before nucleosome assembly. PCNA could be such a coordinator, as it interacts with Polε, Polδ, MutLα, and MutSα through a conserved motif referred to as the PCNA-interacting protein (PIP) box, and is required for MMR initiation (15, 16), replication origin firing, and polymerase processivity (17, 18). In fact, PCNA's roles in nucleotide excision repair and DNA replication are differentially regulated by its inhibitor p21 to specifically block DNA replication, but not nucleotide excision repair, which allows time for damage-responsive repair (19, 20). This mechanism may apply to MMR and DNA replication. However, this supposition has not been verified.

In addition to processing replication-induced biosynthetic errors, the MMR system also recognizes and processes DNA lesions induced by physical and chemical agents. Unlike processing biosynthetic errors, MMR processing of nonmismatched DNA lesions does not remove the lesions; instead, it triggers DNA damage signaling (6, 21). These nonmismatched lesions can arrest the replication machinery and cause replication stress

Author affiliations: [a]Department of Radiation Oncology, University of Texas Southwestern Medical Center, Dallas, TX 75390; and [b]Department of Pathology, University of Texas Southwestern Medical Center, Dallas, TX 75390

Author contributions: J.Z., L.G., and G.-M.L. designed research; J.Z., X.Z., and L.L. performed research; H.-D.L. and D.H.C. contributed new reagents/analytic tools; J.Z., X.Z., L.L., L.G., and G.-M.L. analyzed data; and J.Z., L.G., D.H.C., and G.-M.L. wrote the paper.

The authors declare no competing interest.

This article is a PNAS Direct Submission.

[1]To whom correspondence may be addressed. Email: guo-min.li@utsouthwestern.edu.

This article contains supporting information online at http://www.pnas.org/lookup/suppl/doi:10.1073/pnas.2201738119/-/DCSupplemental.

Published September 26, 2022.

(22, 23), under which stalled forks can be processed into a four-way junction structure called fork reversal or regression, which protects the replication fork from collapsing (24, 25). Regressed fork ends are susceptible to nucleolytic degradation by exonucleases including MRE11 (26), but replication fork degradation can be prevented by fork protecting factors such as BRCA1, BRCA2, FANCD2, and WRN (26–28). Interestingly, MMR proteins constitutively interact with BRCA1 and MRE11 along with other proteins to form a complex named BASC (29). These observations imply that MMR modulates replication fork stability, but the mechanism remains to be investigated.

In this study, we investigated the role of MMR in regulating replication fork progression and stability in mouse embryonic fibroblast (MEF) and endometrial cancer cell (ECC) lines that carry a proline-to-arginine substitution at amino acid 286 (P286R) of Polε (Polε-P286R). This mutation causes a structural change to Polε (30, 31) and results in an ultramutable polymerase (32). We used these cell lines as a tool to naturally generate a high rate of misincorporation without inducing cell toxicity. We demonstrate here that despite high-level recruitment of MutSα to replicating DNA, Polε-P286R cells exhibit an elevated replication progression rate, suggesting that Polε-P286R cells carry out unrestrained DNA replication, i.e., replication progression in Polε-P286R cells has little to do with MMR. However, we surprisingly find that under replication stress induced by hydroxyurea (HU), Polε-P286R cells exhibit vigorous nascent strand degradation in a manner dependent on both MutSα and the 3′-5′ exonuclease MRE11. This degradation causes ssDNA accumulation, double strand breaks (DSBs), and eventually chromosome abnormalities. Therefore, this study has identified an unusual MutSα function in promoting replication fork degradation and genome instability under replication stress.

Results

MMR Does Not Slow Down Replication Progression Catalyzed by Polε-P286R. To determine whether correction of biosynthetic errors by MMR pauses DNA replication, we used two mouse cell lines that carry a heterozygous proline-to-arginine mutation at amino acid 286 (P286R) of Polε (Polε-P286R). These cell lines are MEF cell line A3-6 and ECC line D-1E (32, 33), which are referred to as Polε-P286R MEF and Polε-P286R ECC, respectively. MEF cell line C3-4 and ECC cell line UCS1 (34) were used as Polε wild-type (WT) controls. To determine Polε-P286R–caused mutation frequency, we performed hypoxanthine guanine phosphoribosyl transferase (HPRT) assays in MEF WT C3-4 and Polε-P286R A3-6 cells, and found that Polε-P286R MEF cells displayed a mutation frequency 120-fold higher than WT controls (Fig. 1*A*), consistent with the documented ultramutator phenotype of Polε-P286R (33). Our functional in vitro MMR assay (35) showed that MMR activity in Polε-P286R MEF cells is as active as that of WT MEF cells (*SI Appendix*, Fig. S1 *A* and *B*). Thus, Polε-P286R cells are ideal for testing whether correction of biosynthetic errors by MMR regulates DNA replication progression.

Since MMR is coupled to replication (11, 12) and since the initial MMR event is the recognition of mispaired bases by MutSα or MutSβ, we assessed the binding of MSH2 (the obligating subunit of both MutSα or MutSβ) to replicating DNA/chromatin in Polε-P286R and control cells using bromodeoxyuridine (BrdU) immunofluorescence staining analysis (36). We found that Polε-P286R MEF cells displayed significantly more chromatin/DNA-bound MSH2 than control MEF cells (Fig. 1 *B* and *C*). To further address this finding, we directly visualized chromatin-bound MSH6 by confocal immunofluorescence analysis after cells were preextracted with the cytoskeletal buffer, which removes loosely chromatin-bound proteins before fixing (37). As a positive control, WT MEF cells were treated with *N*-methyl-*N*′-nitro-*N*-nitrosoguanidine (MNNG), which induces O^6-methylguanine DNA adducts specifically recognized by MutSα (6, 21). We indeed observed tightly bound MSH6 in MNNG-treated WT cells (*SI Appendix*, Fig. S1*C*, image 1). However, in the absence of MNNG, tightly bound MSH6 was observed in Polε-P286R MEF cells (*SI Appendix*, Fig. S1*C*, image 2), but not in WT MEF controls (*SI Appendix*, Fig. S1*C*, image 3). More MSH2 and MSH6 were also recovered in the chromatin fraction of Polε-P286R MEF cells than that of control cells (Fig. 1*D*). To determine the level of replication fork–bound MutSα, we labeled cells with BrdU, followed by cross-linking. The cross-linked protein–DNA complexes were pulled down by an MSH6 antibody, and the precipitated DNA was quantified using a NanoDrop Spectrophotometer and directly visualized by an anti-BrdU antibody after slot blotting. The results showed higher DNA concentration and more BrdU-labeled DNA in Polε-P286R MEF cells than in WT controls (Fig. 1 *E* and *F*). We then performed the SILAC (stable isotope labeling of amino acids in cell culture) (38) and iPOND (isolation of protein on nascent DNA) assays (39), followed by quantitative mass-spectrometry (MS) analysis (*SI Appendix*, Fig. S1*D*). This analysis identified MutSα as one of the most enriched proteins at the replication fork, demonstrating fivefold higher MutSα in Polε-P286R MEF cells than WT controls (*SI Appendix*, Fig. S1*E*). Collectively, these observations clearly indicate that more MutSα molecules are recruited to replication forks in Polε-P286R cells than in WT controls.

To test the impact of MMR on replication progression, we measured the replication speed in Polε-P286R MEF and control cells using the DNA fiber assay, in which progressing replication forks are sequentially labeled with thymidine analogs 5-iodo-2′-deoxyuridine (IdU) and 5-chloro-2′-deoxyuridine (CldU), followed by immunostaining (40). To our surprise, Polε-P286R MEF cells exhibited DNA fiber tracts significantly longer than those in control cells (Fig. 1*G*). These results were confirmed in four other MEF cell lines (32), which are WT lines C3-5 and C3-7, and Polε-P286R mutants A3-3 and A3-8 (*SI Appendix*, Fig. S2*A*). Knockdown (KD) of *Msh6* in Polε-P286R MEF cells (*SI Appendix*, Fig. S2*B*) did not alter the replication progression speed, as there was no difference in the DNA fiber tract length between *Msh6*-deficient and *Msh6*-proficient Polε-P286R MEF cells (Fig. 1*H*). Similar results were also observed in three Polε-P286R-*Msh2*$^{-/-}$ ECC cell lines Pms4-4, Pms10-2, and Pms9-3 (*SI Appendix*, Fig. S2 *C* and *D*), as compared with three MMR-proficient Polε-P286R lines A-1E, B-3E, and D-1E (33). Taken together, these results suggest that replication progression, at least for Polε-P286R–catalyzed DNA synthesis, is not controlled by MMR. This may simply reflect the superactive nature of Polε-P286R (30, 31), which can create a relatively long distance between the replisome and the MMR machinery so that the appropriate interplay between these machineries is inhibited.

MutSα Is Required for Stalled Fork Degradation in Polε-P286R Cells. Because the presence of MutSα at replication forks did not slow down the replication progression, we wondered whether the fork-bound MutSα plays a role in regulating replication fork stability. To explore this possibility, we treated cells with aphidicolin (Aph) or HU to induce replication stress (41), followed by measuring DNA fiber lengths. The results showed that Aph or HU treatment significantly reduced the DNA fiber length in

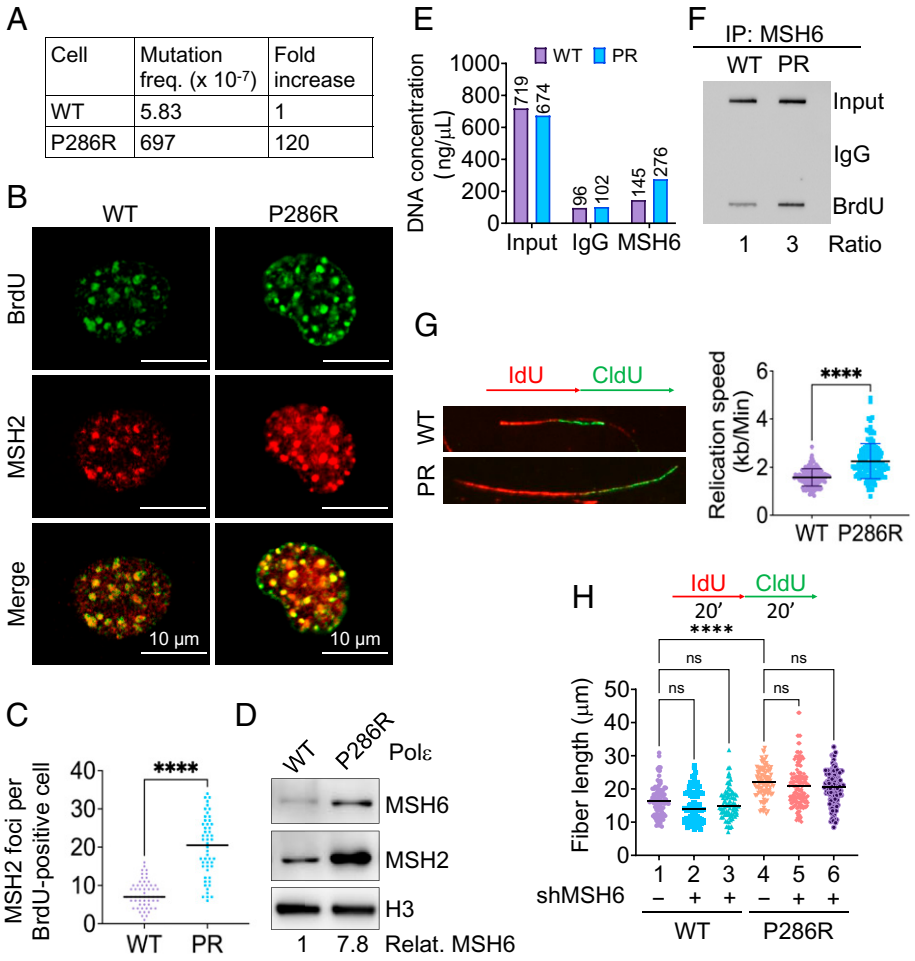

Fig. 1. MMR does not slow down replication progression catalyzed by Polε-P286R. (*A*) HPRT analysis showing increased mutation frequency in Polε-P286R MEF cells. (*B*) Representative immunofluorescence images showing increased recruitment (both foci number and size) of MSH2 to chromatin and high-level MSH2-BrdU colocalization in P286R MEF cells. (*C*) Quantification of MSH2 foci number per nucleus in BrdU positive cells, as shown in *B*. (*D*) Immunoblotting analysis of chromatin-bound MMR proteins in WT and Polε-P286R MEF cells synchronized in S phase. (*E* and *F*) BrdU-ChIP analysis showing DNA immunoprecipitated by an MSH6 antibody (*E*) and amount of immunoprecipitated BrdU-labeled replicating DNA (*F*) in WT and Polε-P286R MEF cells. (*G*) Representative DNA fibers labeled with IdU and CldU analogs (*Left*), as indicated, in WT and Polε-P286R MEF cells. Fiber lengths were measured, and replication speed were calculated (*Right*). (*H*) DNA fiber length in WT and Polε-P286R MEF cells with or without *Msh6* knockdown, as indicated. Statistical analyses were performed using two-tailed unpaired *t* test or one-way ANOVA. SD (SEM) was determined using data from three independent experiments. At least 100 cells or fibers were quantified for nuclear foci/DNA fiber length. Data were considered statistically significant if *P* values were less than 0.0001 (****). For all figures, ns, not significant.

both WT and Polε-P286R MEF cells (Fig. 2 *B* and *C*), but Polε-P286R cells showed greater decrease than control cells (Fig. 2*A*, compare treatments 2 and 6; Fig. 2*B*, compare treatments 3 and 6), indicating that Polε-P286R cells are more sensitive to replication stress. Since replication stress induces regressed forks, which are vulnerable to degradation by nucleases (42), we examined the potential impact of MutSα on replication fork integrity in Polε-P286R cells in the presence or absence of MutSα under three different DNA fiber labeling conditions: 1) HU (4 mM) was added to culture after consecutive incubations with IdU and CldU, and the ratio of the tract length between CldU and IdU was then calculated (Fig. 2 *C*–*E*); 2) HU and CldU were added to the culture after IdU treatment, and the tract length of IdU was quantified (Fig. 2*F*); 3) HU was added to the culture between IdU and CldU pulses and the IdU tract length was measured (Fig. 2*G*). Interestingly, in all cases, HU treatment led to vigorous degradation of the nascent DNA tract in Polε-P286R cells but not in WT cells. The degradation is MutSα dependent, as *Msh6* knockdown (*SI Appendix*, Fig. S2*B*) in MEF cells (Fig. 2 *C* and *D*, treatment 4) or *Msh2* knockout (KO) (*SI Appendix*, Fig. S2*C*) in ECC cells (Fig. 2*E*, treatment 3) blocked the degradation of the CIdU tract in Polε-P286R cells. Similar results were observed in the other two labeling conditions, i.e., fork degradation occurs in MutSα-proficient Polε-P286R cells, but diminished when MutSα was depleted (Fig. 2 *F* and *G*, compare treatments 6 and 8). Collectively, these results reveal a MutSα-dependent degradation of nascent strands under the condition of replication stress.

MMR-Dependent Fork Degradation Requires MRE11 and RAD51. The 3′ to 5′ exonuclease MRE11, a MutSα-interacting protein (43, 44), has been shown to catalyze HU-induced replication fork degradation, particularly in BRCA1/2-deficient cells (28, 45, 46). To determine whether MRE11 is involved in the MutSα-dependent degradation of nascent strands in Polε-P286R cells, we treated cells with MRE11-specific inhibitor mirin and analyzed the nascent DNA tract ratio in HU-treated Polε-P286R cells with or without MSH6 expression. We found that mirin treatment restored the nascent strand length in Polε-P286R cells with or without a functional MutSα to the level usually seen in WT cells (Fig. 3*A*, compare treatment 1 with treatments 2 and 4; *SI Appendix*, Fig. S3*A*). This observation supports the idea that MRE11 is responsible for the MutSα-dependent degradation of nascent strands in Polε-P286R cells. To confirm this result,

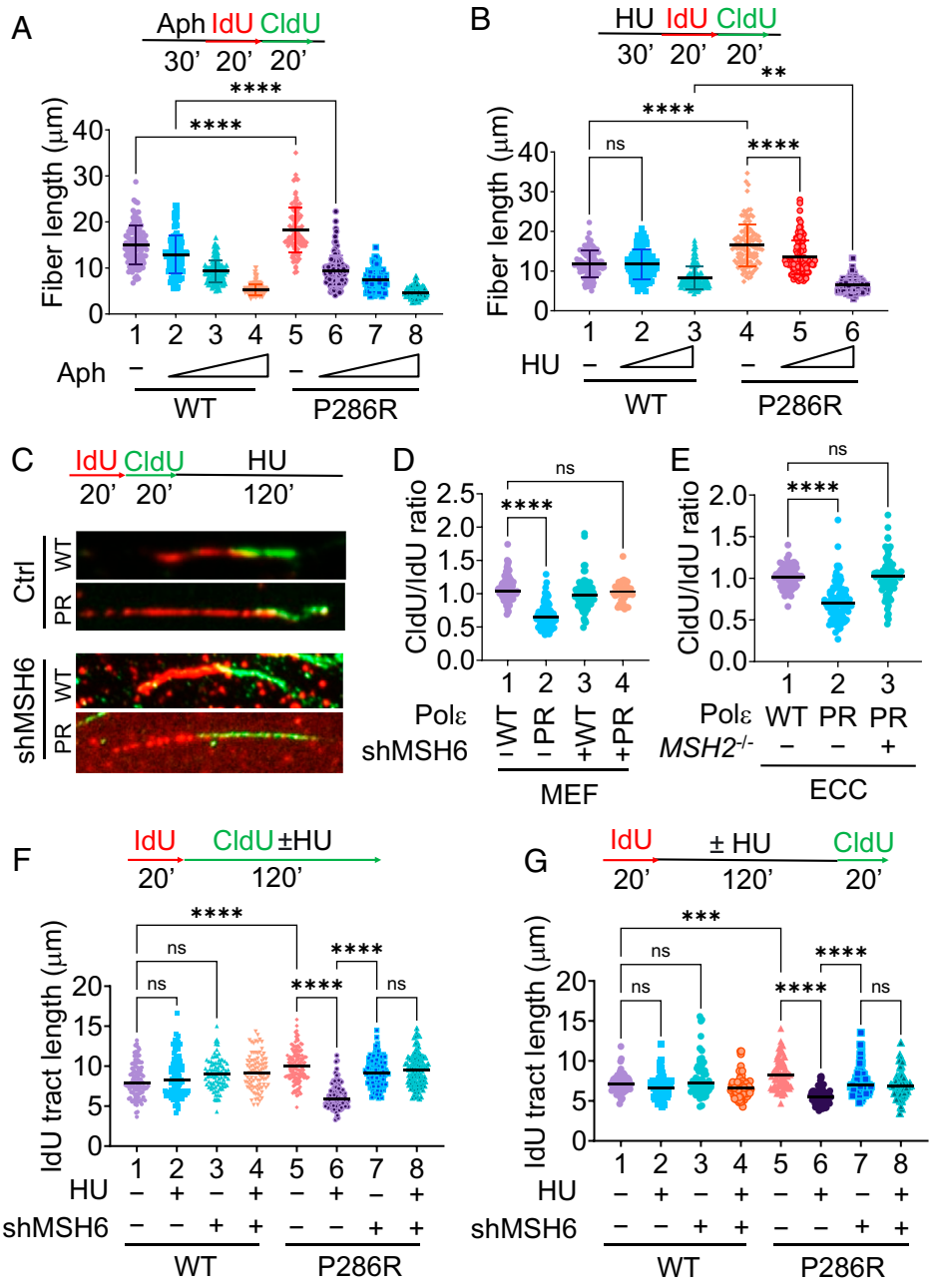

Fig. 2. Polε-P286R cells exhibit MutSα-dependent nascent strand degradation. (*A* and *B*) DNA fiber lengths in WT and Polε-P286R MEF cells treated with various concentrations of Aph (0 nM, 100 nM, 1 μM, and 20 μM) or HU (0 μM, 50 μM, and 1 mM) prior to labeling with IdU and CldU, as indicated. (*C*) Representative images of DNA fiber assays showing MMR-dependent fork degradation. Cells were sequentially labeled with IdU and CldU, followed by HU chasing and DNA fiber visualization by a Zeiss Axioimager microscope. (*D and E*) Determination of nascent strand degradation using the tract length ratio of CldU:IdU in WT and Polε-P286R MEF with or without *Msh6* knockdown and Polε-P286R ECC with or without *Msh2* knockout, as indicated. (*F* and *G*) IdU tract length in WT and Polε-P286R MEF cells with or without *Msh6* knockdown in the presence and absence of HU, as indicated. The HU treatment was either after IdU labeling (*F*) or between IdU and CldU incubations (*G*). $^{**}P < 0.01$; $^{***}P < 0.001$; $^{****}P < 0.0001$.

we performed immunofluorescence analysis to determine the recruitment of MRE11 to the damage sites. We observed significantly elevated foci formation of MRE11 in Polε-P286R cells compared to WT cells, both in the presence and absence of HU treatment (Fig. 3*B* and *SI Appendix*, Fig. S3*B*). However, significantly less MRE11 was recruited in *Msh6*-depleted Polε-P286R cells (Fig. 3*B* and *SI Appendix*, Fig. S3*B*). Our SILAC analysis also identified fourfold higher MRE11 at the replication fork of Polε-P286R cells than WT cells (*SI Appendix*, Fig. S1*E*). These findings suggest that both the MRE11-catalyzed nascent strand degradation and chromatin localization depend on MutSα.

DNA2 and exonuclease 1 (Exo1) also carry out nascent strand degradation (47, 48). To determine their involvement in the MutSα-dependent fork degradation, we analyzed the nascent DNA tract ratio in cells treated with C5, a DNA2-specific inhibitor (Fig. 3*C*) or cells with *Exo1* knockout (*SI Appendix*, Fig. S3*C* and Fig. 3*D*) and found that the MutSα-dependent nucleolytic degradation remains the same in Polε-P286R MEF cells. We conclude that both DNA2 and Exo1 are not involved in MutSα-dependent nascent strand degradation in Polε-P286R cells.

MRE11-mediated fork degradation occurs upon fork reversal, which is dependent on RAD51 (26, 28). To determine whether RAD51 is also required for the MMR-dependent fork degradation in Polε-P286R cells, we knocked down *Rad51* (*SI Appendix*, Fig. S3*D*) in both WT and Polε-P286R MEF cells

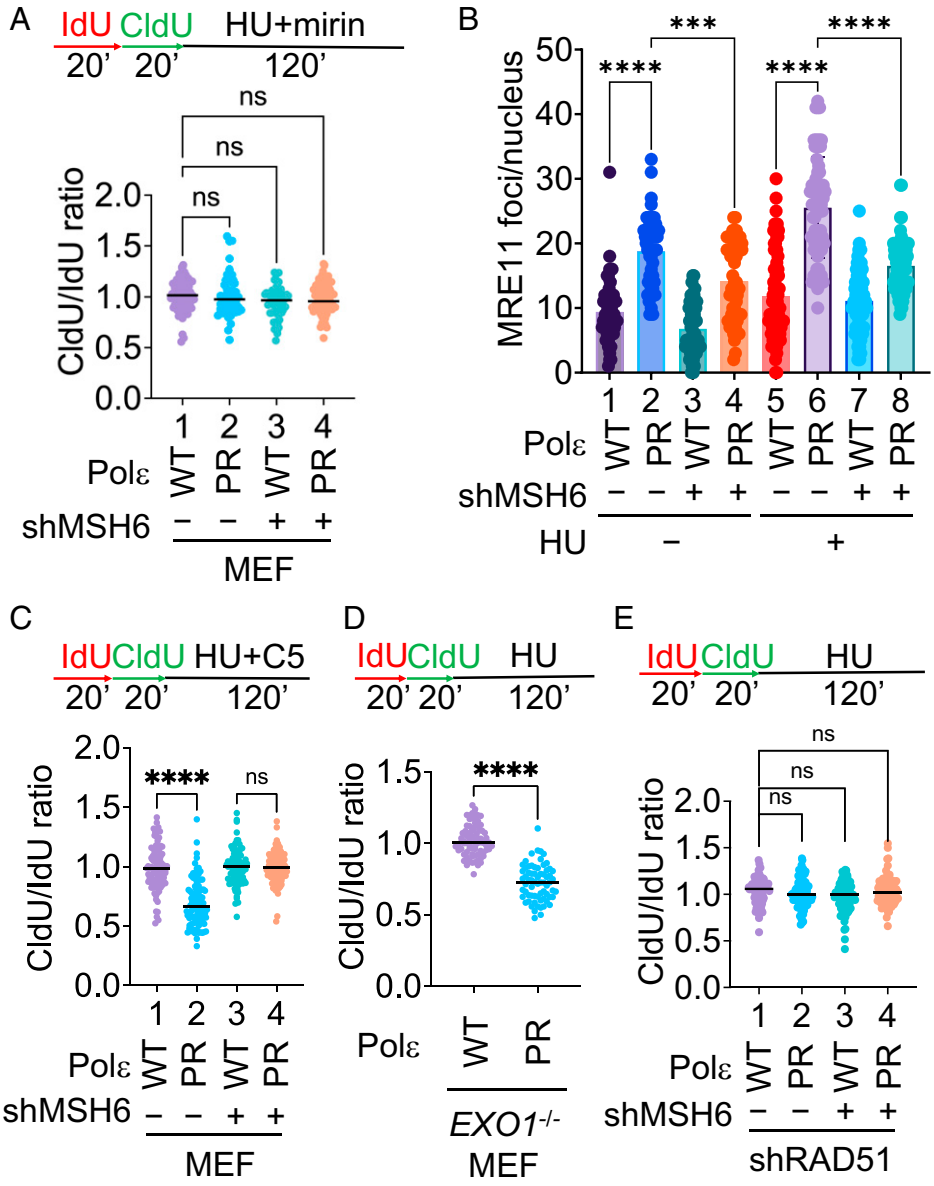

Fig. 3. MRE11 and RAD51 are required for MMR-dependent fork degradation in Polε-P286R cells. (*A*) Determination of CldU/IdU tract length ratio in HU-treated WT and Polε-P286R MEF cells with or without *Msh6* knockdown in the presence of MRE11 inhibitor mirin (50 μM). (*B*) Quantification of MRE11 foci per nucleus in WT and Polε-P286R MEF cells with or without *Msh6* knockdown in the presence or absence of HU, as indicated. (*C*) Determination of CldU/IdU tract length ratio in HU- and DNA2 inhibitor C5-treated WT and Polε-P286R MEF cells with or without *Msh6* knockdown, as indicated. (*D*) Determination of CldU/IdU tract length ratio in *Exo1*-knockout WT and Polε-P286R MEF cells after HU treatment. (*E*) Determination of CldU/IdU tract length ratio in *Rad51*-knockdown WT and Polε-P286R MEF cells with or without *Msh6* knockdown, as indicated. ***$P < 0.001$; ****$P < 0.0001$.

and analyzed their DNA fiber tract length. As shown in Fig. 3*E*, depleting *Rad51* abolished MutSα-dependent nascent strand degradation in Polε-P286R MEF cells, as the CldU/IdU tract length ratio remains at 1 when *Rad51* was depleted, regardless of the presence of MSH6 (lanes 2 and 4). This suggests that fork reversal by RAD51 is also a prerequisite for MutSα-dependent nascent strand degradation in Polε-P286R cells.

MutSα Blocks Recruitment of Fork Protection Factors. To understand the mechanism by which MutSα promotes MRE11-catalyzed nascent strand degradation, we performed the iPOND-MS assay, using thymidine chase as a control (*SI Appendix*, Fig. S4*A*). As expected, MMR components such as MSH2, MSH6, MLH1, and PCNA were all recovered on nascent DNA strands in both WT and Polε-P286R cells (*SI Appendix*, Fig. S4 *B* and *C*). However, we found that several proteins involved in the FANCD2-BRCA pathway, including FANCD2 and BRCA1, were preferentially enriched in WT MEF cells (Fig. 4*A*), indicating reduced association of these proteins with the replication fork in Polε-P286R cells.

FANCD2 and BRCA1 stabilize replication forks under replication stress by protecting DNA ends from MRE11-catalyzed degradation (42, 49). We speculated that binding of MutSα at replication forks in HU-treated Polε-P286R cells inhibits the recruitment of FANCD2/BRCA1, which subsequently allows MRE11 to degrade the nascent strands. To test this idea, we examined the interaction of MSH6 or FANCD2 with BrdU-labeled nascent DNA in WT and Polε-P286R MEF cells after HU treatment, as well as *Msh2*-proficient and deficient P286R ECC cells. Numerous foci colocalizations between MSH6 and BrdU were observed in MutSα-proficient cells (Fig. 4*B*, images 17 and 18), but there were significantly more colocalized BrdU-MSH6 foci in Polε-P286R cells than in WT controls (Fig. 4*C*). Interestingly, FANCD2 foci formation (Fig. 4*B*, image 14 and

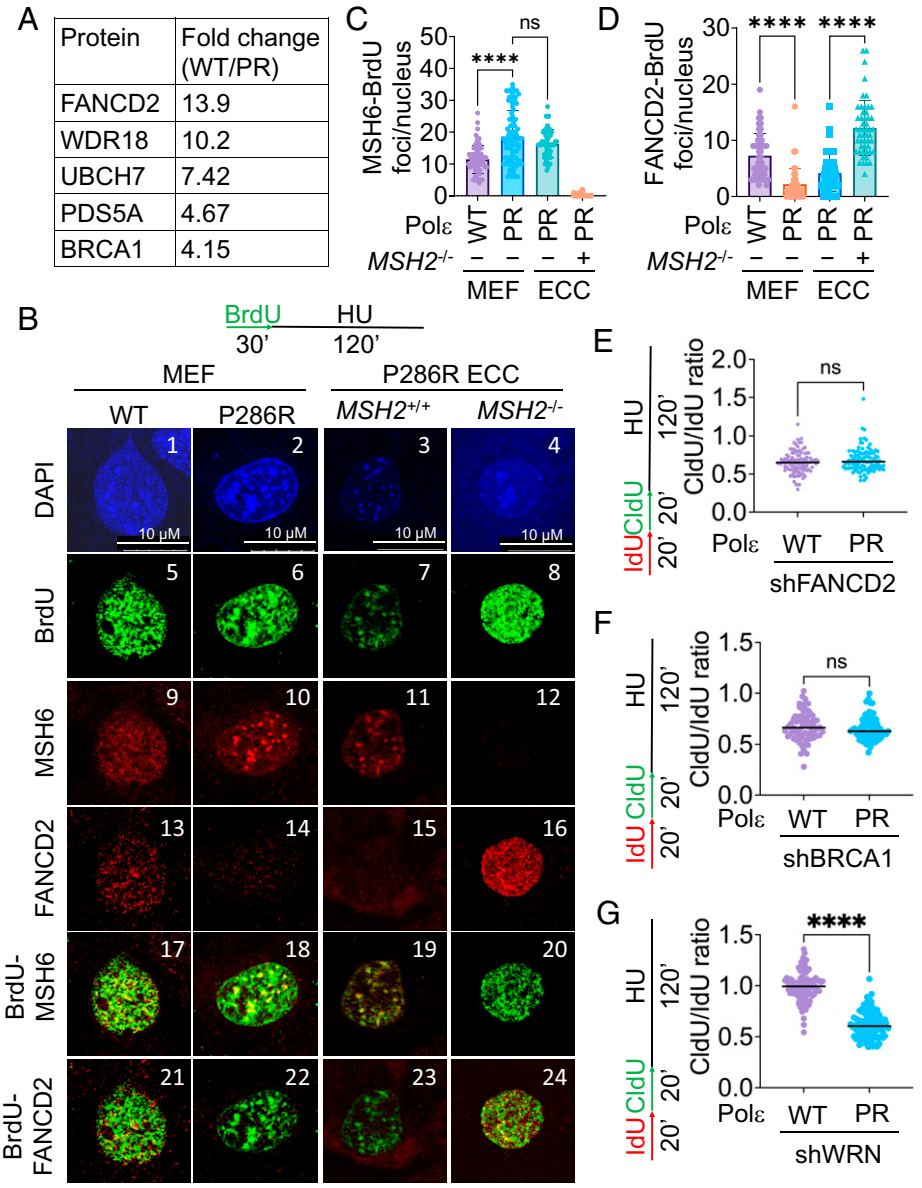

Fig. 4. MutSα promotes nascent strand degradation by blocking recruitment of fork protection factors. (*A*) Selected differentially recruited proteins pulled down from replication fork by iPOND in WT and Polε-P286R MEF cells and identified by mass spectrometry. Protein abundance was normalized by histone and shown as WT/P286R ratio. (*B*) Representative immunofluorescence images of FANCD2 and MSH6 in HU-treated MEF and ECC cells labeled with BrdU, which show mutual exclusive nature on chromatin between FANCD2 and MSH6/MSH2. (*C*) Quantification of colocalized MSH6-BrdU foci per nucleus in MEF and ECC cells, as indicated. (*D*) Quantification of FANCD2-BrdU foci number per nucleus in MEF and ECC cells, as indicated. (*E*) CldU/IdU tract length ratio in HU-treated *Fancd2*-knockdown WT and Polε-P286R MEF cells. (*F*) CldU/IdU tract length ratio in HU-treated *Brca*-knockdown WT and Polε-P286R MEF cells. (*G*) CldU/IdU tract length ratio in HU-treated *Wrn*-knockdown WT and Polε-P286R MEF cells. ****$P < 0.0001$.

15) and foci colocalizations between FANCD2 and BrdU (Fig. 4*B*, image 22 and 23; Fig. 4*D*) were rarely detected in MMR-proficient Polε-P286R MEF and ECC cells. However, when *Msh2* was depleted in Polε-P286R ECC cells, obvious colocalizations between FANCD2 and BrdU were observed (Fig. 4*B*, image 24; Fig. 4*D*). These results suggest that MutSα recruitment to the newly synthesized DNA, especially in Polε-P286R cells, blocks the recruitment of FANCD2 to replication forks to execute its protection function, leading to fork degradation by MRE11. These results were further confirmed by determining binding of FANCD2 to EdU-labeled newly synthesized DNA (*SI Appendix*, Fig. S5 *A* and *B*). Consistent with the role of FANCD2 and BRCA1 in protecting replication forks (49), MEF cells depleted of *Fancd2* (*SI Appendix*, Fig. S5*C*) or *Brca1* (*SI Appendix*, Fig. S5*E*), regardless of WT or Polε-P286R, exhibited nascent strand degradation, as the CldU/IdU track length ratio is less than 1 (Fig. 4 *E* and *F* and *SI Appendix*, Fig. S5 *D* and *G*). However, nucleolytic degradation was not observed in WT MEF cells depleted of *Wrn* (Fig. 4*G* and *SI Appendix*, Fig. S5 *F* and *G*), which codes another fork-protecting factor WRN.

MutSα-Dependent Fork Degradation Leads to DNA Breaks and Chromosome Instability. We postulated that MutSα-dependent nascent strand degradation by MRE11 generates single stranded DNA (ssDNA), which is protected by RPA. We therefore analyzed RPA foci formation in Polε-P286R cells in the presence or absence of MutSα. As shown in Fig. 5*A*, increased numbers of RPA foci were observed in Polε-P286R MEF cells under unperturbed conditions (compare images 1 and 2). The increase in RPA foci was significantly higher in Polε-P286R MEF cells than in WT controls (Fig. 5*A*, compare images 5 and 6) when they were treated with HU, but MSH6 knockdown decreased the

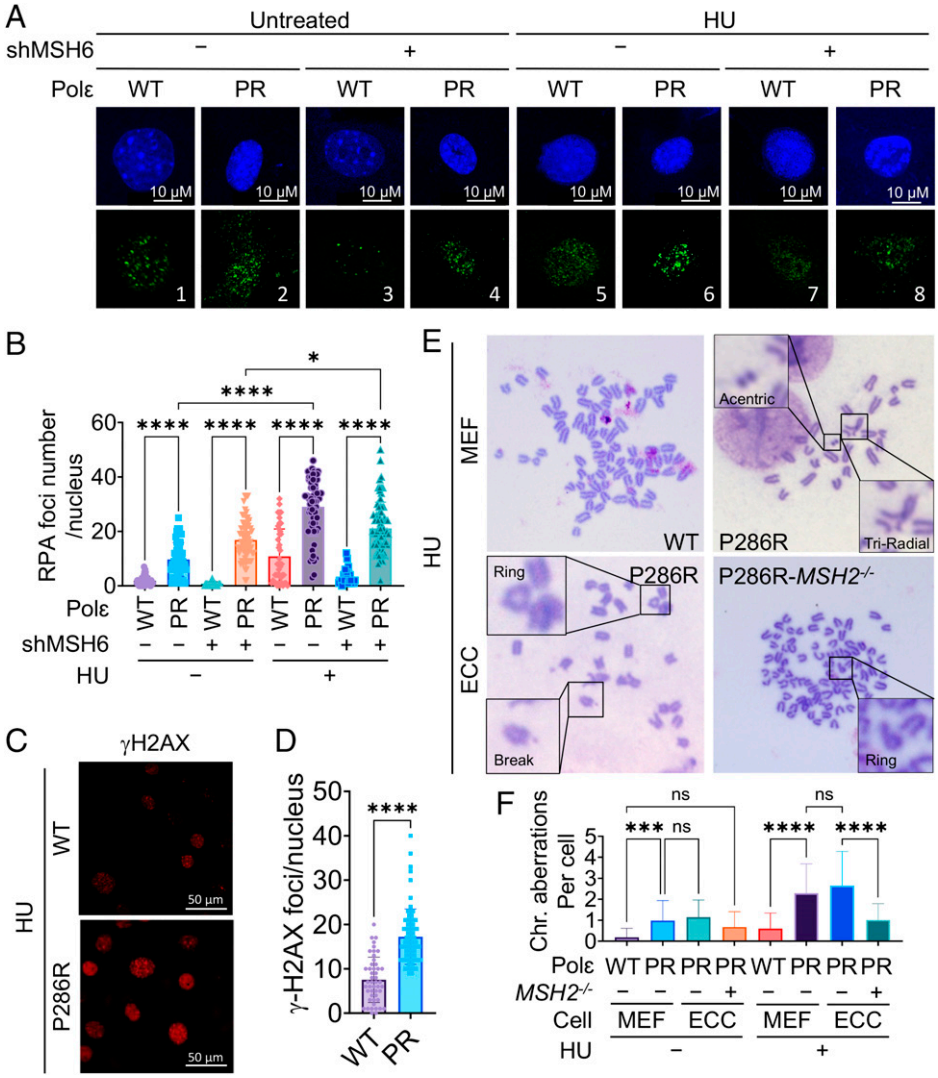

Fig. 5. MMR-dependent nascent strand degradation induces genomic instability. (*A*) Representative immunofluorescence images from various cells showing more RPA foci in Polε-P286R cells under replication stress in a manner dependent on MSH6. (*B*) Quantification of RPA foci per nucleus in MEF cells, as shown in *A*. (*C*) Representative immunofluorescence images showing increased γH2AX foci number in Polε-P286R MEF cells after HU treatment. (*D*) Quantification and comparison of γH2AX foci in WT and Polε-P286R MEF cells, as shown *C*. (*E*) Chromosome spreading analysis to determine chromosomal aberrations in WT and Polε-P286R MEF cells as well as in *Msh2*-proficient and deficient Polε-P286R ECC cells after HU treatment. Aberrations were enlarged and labeled, as indicated. (*F*) Average number of chromosomal aberrations per cell in two pairs of MEF cells (WT: C3-4 and C3-7; PR: A3-6 and A3-8) and two pairs of *MSH2*-proficient (A-1E and D-1E) and deficient Polε-P286R (Pms4-4 and Pms9-3) ECC cells. Essentially, equal numbers of cells were chosen between duplicated cells in each cell type, with $n = 66$ (WT MEF), 63 (PR MEF), 60 (*MSH2*-proficient PR), 52 (*MSH2*-deficient PR), 54 (WT MEF), 64 (PR MEF), 50 (*MSH2*-proficient PR), and 51 (*MSH2*-deficient PR). *$P < 0.05$; ***$P < 0.001$; ****$P < 0.0001$.

RPA level in P286R MEF cells (Fig. 5*A*, compare images 6 and 8; Fig. 5*B*). These results are consistent with our prediction that the MutSα-dependent nascent strand degradation produces ssDNA. Since persistent ssDNA induces DSBs at the replication forks (50), we measured the number of γH2AX foci (a DSB marker) in HU-treated WT and Polε-P286R MEF cells by immunofluorescence analysis. Indeed, we observed a significantly higher level of γH2AX foci in Polε-P286R MEF cells than in WT controls (Fig. 5 *C* and *D*), suggesting that MutSα-dependent nascent strand degradation leads to DSBs.

Nucleolytic degradation under replication stress can induce chromosomal aberrations in cells defective in fork protection (28). We therefore performed chromosome spread analysis and indeed observed increased chromosome aberrations, including acentric fragments, radial, triradial, and breaks in unperturbed Polε-P286R MEF cells, as cells occasionally undergo replication stress under culture conditions (*SI Appendix*, Fig. S6*A*). This effect was partially restored when MutSα was depleted (*SI Appendix*, Fig. S6*A*). Treatment with HU significantly enhanced the severity of chromosome instability, especially in Polε-P286R cells, but the level of chromosome abnormality was reduced when *Msh2* was depleted (Fig. 5 *E* and *F*), indicating that the observed chromosome abnormalities are MutSα dependent. Increased amount of chromosome abnormalities in Polε-P286R cells were further confirmed in two other Polε-P286R MEF cell lines A3-3 and A3-8, as compared with WT MEF lines C3-4 and C3-5 (*SI Appendix*, Fig. S6 *B* and *C*). It is worth noting that Polε-P286R cells appear to escape from colcemid-induced spindle assembly checkpoint (SAC), as less than 1% of Polε-P286R cells displayed metaphase after colcemid block (in comparison to 20% observed in WT cells), making chromosome spread in Polε-P286R cells difficult. This is likely due to the lack of FANCD2 binding in nascent DNA, as FANCD2 is required for SAC and proper mitosis (51). Overall, these findings indicate that MutSα binding at the replication fork leads to MRE11-mediated fork degradation, which eventually leads to chromosome instability.

Discussion

In this study, we attempted to understand, but fail to address, how MMR regulates replication progression by repairing misincorporated nucleotides generated by Polε-P286R, which is probably due to the fact that the superactive Polε-P286R (31) may have created a distance barrier for physical interaction between the MMR system and the replication machinery. However, we unexpectedly discovered a hitherto unidentified MMR function to promote nascent strand degradation at stalled replication forks.

As a replication-coupled DNA repair machinery (11, 12), MMR is well known for its role in removing biosynthetic errors during DNA replication, thereby ensuring replication fidelity (2–4). In addition, the MMR system also recognizes and processes chemically and physically modified nonmismatched DNA adducts (6). However, the latter function does not remove the adducts from DNA, but activates the DNA damage response (DDR) pathway (2, 6, 23). Here, we have identified another replication-associated MMR function. Under replication stress, mismatch-bound MutSα blocks fork protection factors FANCD2 and BRCA1 from loading to replication forks and promotes MRE11's binding to the fork, probably through the physical interaction between MutSα and MRE11 (43, 44). However, the MutSα-dependent MRE11-catalyzed excision, which is stimulated in cells with error-prone DNA synthesis, degrades the nascent DNA strand, leading to DNA breaks and chromosome abnormalities. While the error correction and DDR activities of the MMR system promote genome stability, the MutSα-dependent fork degradation function induces DNA breaks and genome instability.

We observed increased MutSα binding at stalled replication forks in Polε-P286R (Fig. 4 *B* and *C*). The simplest explanation for this is that Polε-P286R induces multiple mismatches at the replication fork. Although Polε-P286R cells display an elevated mutation frequency (7×10^{-5}, Fig. 1*A*), which is consistent with a previous study (33), the calculated number of mutations is ∼7/100,000 bp, suggesting that there may be only one mismatch at a replication fork. Thus, the above explanation is not appropriate for the observed increase in MutSα level at replication forks. However, this could be attributed to MutSα's mismatch binding and sliding activities (52). It is well accepted that MutSα identifies mismatches by active sliding around the DNA helix; but once it locates a mismatch, the MutSα protein stays mismatch bound until the mismatch is removed (53). Thus, binding of MutSα to a mismatch at stalled replication forks can block the way of other sliding MutSα molecules, resulting in accumulation of several MutSα proteins at the mismatch site. In addition, replication fork reversal can merge mismatches originally located in the leading and lagging strands into the reversed heteroduplex, which enhances the local mismatch concentration and provokes loading of multiple MutSα proteins to the stalled replication fork. These possibilities require further investigations.

Targeting replication stress for synthetic lethality has merged as a potential strategy for cancer therapy, but drug resistance associated with this approach has been a concern (54). The newly identified MMR function may have provided a direction for the replication stress–targeted therapy. We have recently shown that the responsiveness of *MLH1*-deficient tumors to immunotherapy relies on the tumors' ability to not only generate a large quantity of neoantigens, but also activate the cGAS-STING innate immune signaling pathway (55, 56). This is because defects in MLH1, a subunit of MutLα (57), results in the loss of MutLα-specific regulation of Exo1 during DNA repair so that Exo1 can carry out uncontrolled DNA excision. This causes increased DNA breaks and chromosomal abnormalities, leading to accumulation of cytosolic DNA and activation of the cGAS-STING pathway (55). We observed similar phenomena in Polε-P286R cells in a manner dependent on MutSα and replication stress, which include the formation of dsDNA breaks and chromosome aberrations. Thus, the MutSα-dependent MRE11-catalyzed nascent strand degradation in Polε-P286R cells may activate the cGAS-STING pathway. This prediction is well supported by a recent study showing that stalled replication fork degradation in FANCD2-deficienct cells leads to accumulation of cytosolic DNA and activation of the cGAS-STING pathway (58). If this indeed occurs in replication stalled cancer cells, the replication stress-targeted therapy should be combined with immunotherapy, i.e., initial chemotherapy to induce stalled replication fork and cGAS activation, followed by immunotherapy. Further studies will need to verify the efficacy of this combined treatment for cancers with an active MutSα, particularly those defective in replication fork protection factors such as FANCD2, BRCA1, and BRCA2.

In summary, we show that under the condition of replication stress, fork-bound MutSα promotes MRE11-catalyzed nascent strand degradation by blocking the recruitment of fork protecting factors FANCD2 and BRCA1 to replication fork. This MutSα-dependent fork degradation, which is stimulated by Polε-P286R–induced misincorporations, causes DNA breaks and chromosome instability. Therefore, our study has identified a function of MMR in the replication stress response, and the finding will likely impact cancer therapy.

Materials and Methods

Cell Lines and Cell Culture. Three pairs of MEF lines (Polε-WT lines C3-4, C3-5, and C3-7; and Polε-P286R lines A3-3, A3-6, and A3-8) and three pairs of mouse ECC lines (Polε-P286R lines A-1E, B-3E, and D-1E; and Polε-P286R-*Msh2*$^{-/-}$ lines Pms4-4, Pms9-3, and Pms10-2) (32, 33) were used in this study. A *Pten* mutant ECC cell line UCS1 (34), which carries a low mutation frequency, was used as the Polε-WT ECC control. C3-4 and A3-6 MEF cells were used to create gene-specific KO or KD derivatives *Msh6*-KD C3-4, *Rad51*-KD C3-4, *Fancd2*-KD C3-4, *Msh6*-KD A3-6, *Rad51*-KD A3-6, *Fancd2*-KD A3-6, and *Exo1*-KO A3-6. The *Msh2*-KO PMS4-4 ECC cell line was generated previously (33). Cells were grown in Dulbecco's Modified Eagle Medium (DMEM) (SH30285.01, HyClone) supplemented with 10% fetal bovine serum, 10% GlutaMax, and 1× penicillin/streptomycin. More detailed information in cell lines and culture is presented in *SI Appendix, Materials and Methods*.

To ensure that all experiments used cells with minimum cell passages and relatively similar genetic background/phenotype, an early passage (∼20) P286R cell line (i.e., MEF lines A3-3, A3-6, and A3-8; Polε-P286R ECC lines A-1E, B-3E, and D-1E; and Polε-P286R-*Msh2*$^{-/-}$ ECC lines Pms4-4, Pms9-3, and Pms10-2) was expanded to obtain 20 aliquot vials, which were stored in liquid nitrogen for use. All experiments in this study started with cells in one of the expanded vials, which had a passage number of ∼30.

In Vitro MMR Assays. In vitro MMR assays (35) were performed in a 20-μL reaction containing 100 ng G-T mismatched DNA (*SI Appendix*, Fig. S1), 25- to 75-μg nuclear extracts, 10 mM Tris-HCl (pH 7.5), 5 mM $MgCl_2$, 1.5 mM Adenosine triphosphate (ATP), 0.1 mM Deoxyribonucleotide triphosphates (dNTPs), and 110 mM KCl. The reaction mixtures were assembled on ice, incubated at 37 °C for 15 min, and terminated by proteinase K digestion. DNA products were recovered by phenol extraction and ethanol precipitation. After digestion with *Pst*I, *Bgl*I, and *Nsi*I (repair-scoring enzyme), DNA products were separated by a 6% polyacrylamide gel and detected by Southern hybridization using a ^{32}P-label probe and visualized by a GE Healthcare Typhoon Phosphor Imager.

HPRT Assay. HPRT mutability assays were performed as described previously (59). Cells (1×10^5) were seeded in triplicate 100-mm Petri dishes for 12 h and fed with complete medium containing 15 μM freshly prepared 6-thioguanine

(6-TG). Plating efficiency was determined by seeding 1×10^3 cells without 6-TG. After 5 d of incubation, cell clones were cultured in 6-TG–free complete medium for 10 more days before staining with 0.05% crystal violet. The mutation frequency was determined by dividing the number of 6-TG–resistant colonies by the total number of cells plated after correcting for their colony-forming ability.

Immunofluorescence Analysis. To detect MSH2, MSH6, or FANCD2 foci, cells were incubated with 50 μM BrdU on sterile glass for 1 h, followed by 15-min fixation with 4% paraformaldehyde and denaturation with HCl. To detect FANCD2-EdU foci, cells were labeled with EdU for 20 min, followed by a 1-h click reaction. For MRE11, RPA, or γ-H2AX foci detection, cells were treated with HU and fixed with 4% paraformaldehyde and permeabilized with 0.25% Triton X-100. In all cases, cells were incubated with a primary antibody overnight, and a secondary antibody for 1 h. Slides were mounted and protein interests were visualized using a Leica confocal microscope. Images were analyzed with NIH ImageJ software (*SI Appendix, Materials and Methods*).

DNA Fiber Assay. A DNA fiber assay was performed as previously described (40). To detect fork progression, cells were incubated consecutively with 50 μM IdU (I7125, Sigma) and 250 μM CldU (C6891, Sigma) for 20 min. To determine fork integrity, cells were either incubated with 50 μM IdU followed by 4 mM HU and 250 μM CldU or consecutively labeled with IdU and CldU, followed by HU treatment. After IdU and/or CldU labeling, cells were harvested and DNA fibers were spread on microscopy slides, followed by fixation with 3:1 methanol:acetic acid and denaturation with 2.5 M HCl. Slides were then incubated with a primary antibody and then a secondary antibody. Fiber images were obtained using a Zeiss Axio Imager fluorescence microscope. Fiber lengths were measured manually using the Zeiss Zen Pro software. At least 150 fibers were quantified for each sample.

SILAC, iPOND, and Mass Spectrometry Analysis. The SILAC-iPOND analysis was performed as previously described (38, 39). A total of 2×10^8 cells were used in this analysis. P286R MEF cells (2×10^8) were cultured in "light" medium containing [$^{12}C^{14}N$]-L-lysine and [$^{12}C^{14}N$]-L-arginine, and WT MEF cells were cultured in "heavy" medium containing [$^{13}C^{15}N$]-L-lysine [$^{13}C^{15}N$]-L-arginine. After more than 99% cells were labeled with isotopes, equal amounts of WT, and P286R cells were incubated with EdU for 10 min. Upon cross-linking with 1% formaldehyde, the isotope-labeled WT and P286R MEF cells were combined to perform the click reaction in the presence of copper to conjugate biotin to EdU, followed by streptavidin bead pulldown. Proteins captured were then dissolved on sodium dodecyl-sulfate polyacrylamide gel electrophoresis (SDS-PAGE)/ and subjected to MS analysis at the University of Texas Southwestern Proteomics Core. Raw MS data files were analyzed using Proteome Discoverer v2.4 SP1 (Thermo), with peptide identification performed using Sequest HT searching against the mouse reviewed protein database from UniProt (downloaded January 28, 2022, 17,062 sequences). Fragment and precursor tolerances of 10 ppm and 0.6 Da were specified, and three missed cleavages were allowed. Carbamidomethylation of Cys was set as a fixed modification, with oxidation of Met, [$^{13}C^{15}N$]-L-lysine [$^{13}C^{15}N$]-L-arginine set as variable modifications. The false-discovery rate (FDR) cutoff was 1% for all peptides. Protein abundances were determined based on the sum of the peak intensities for all peptides matched to that protein.

Nonlabeled iPOND was performed similarly, except without isotope labeling. Briefly, cells were labeled with EdU for 10 min and chased with thymidine for 60 min (for sample #3). All samples were fixed with 1% formaldehyde for 20 min at room temperature and quenched with glycine, followed by the click reaction and streptavidin bead pulldown. Proteins captured were resolved on SDS/PAGE before MS analysis. Protein enrichments were calculated by normalizing each sample to the histone H3 level. The fold of enrichment for individual proteins on the replication fork was calculated by the amount of EdU sample divided by those of the thymidine chase sample. Fork-enriched proteins that are differentially recruited in WT cells in comparison to those in Polε-P286R cells were further compared with the above-mentioned normalized fork-enriched ones.

The LC-MS/MS data has been uploaded to MassIVE, with accession number MSV000090330 (https://massive.ucsd.edu/ProteoSAFe/dataset.jsp?task=a1d6ba03f04a40979393117418bee2c5).

Chromosome Spread Analysis. Chromosome spread analysis was performed as described (55). Briefly, cells were treated with or without 4 mM HU overnight, followed by incubation with 0.1 μg/mL colcemid for 4 h. Cells were then swelled in 75 mM KCl at 37 °C for 15 min, and subjected to fixation with 3:1 methanol:acetic acid and incubation at −20 °C overnight. Chromosomes were then spotted on slides and stained with 5% Giemsa staining solution and analyzed under a Zeiss Axio Imager 2 microscope with 100×/1.4 oil objective. At least 50 cells were counted to determine chromosome aberrations.

Determination of Gene Knockdown/Knockout by qRT-PCR. When a quality antibody (e.g., Exo1 and BRCA1) was not available to detect protein expression in knockout/knockdown cells, we performed qRT-PCR to detect mRNA expression. Total mRNA was extracted using TRIzol reagent (15596018, Thermo Fisher Scientific), purified by ethanol precipitation, and dissolved in 0.1% diethylpyrocarbonate (DEPC)-treated water. A total of 1 μg RNA was used to perform reverse transcription using the qScript cDNA Synthesis Kit (Quantabio). One-tenth of the reverse transcription products was used for qRT-PCR using PerfeCTa SYBR Green SuperMix (Quantabio) and a CFX Connect Real-Time Cycler (Bio-Rad). The cDNA of the GAPDH gene was used as a control for normalization. mRNA expression level was quantified by the $2^{-\Delta\Delta Cq}$ (Livak) method. Primers used for qRT-PCR are available upon request.

Statistical Analysis. Student's *t* test (two-tailed, unequal variance) and one-way analysis of variance (ANOVA) were used to compare two datasets and more than two datasets, respectively. At least three independent experiments were performed, and at least 50 cells or 150 fibers were quantified for nuclear foci or DNA fiber length, respectively. Data were considered statistically significant if *P* values were less than 0.05. Analysis was performed by GraphPad Prism 9 software.

Data, Materials, and Software Availability. All study data are included in the article and/or supporting information. Primers used for qRT-PCR are available upon request.

ACKNOWLEDGMENTS. We thank Drs. Anthony Davis and Jan Erzberger for helpful comments during the course of the study; Drs. Junhong Guan, Jinzhen Guo, Janice Ortega, and Xiao Sun in the G.-M.L. laboratory for experimental help; and Dr. Ileana C. Cuevas for sharing the UCS1 cell line. We also thank the University of Texas Southwestern Medical Center Proteomics Core and Dr. Andrew Lemoff for MS analysis. The work was supported in part by a grant from the Cancer Prevention and Research Institute of Texas (RR160101, to G.-M.L.) and National Cancer Institute Grant R01CA237405 (to D.H.C.). G.M.-L. is a CPRIT Scholar in Cancer Research and the holder of the Reece A. Overcash, Jr. Distinguished Chair for Research on Colon Cancer.

1. S. Waga, B. Stillman, The DNA replication fork in eukaryotic cells. *Annu. Rev. Biochem.* **67**, 721–751 (1998).
2. G. M. Li, Mechanisms and functions of DNA mismatch repair. *Cell Res.* **18**, 85–98 (2008).
3. S. D. McCulloch, T. A. Kunkel, The fidelity of DNA synthesis by eukaryotic replicative and translesion synthesis polymerases. *Cell Res.* **18**, 148–161 (2008).
4. P. Modrich, R. Lahue, Mismatch repair in replication fidelity, genetic recombination, and cancer biology. *Annu. Rev. Biochem.* **65**, 101–133 (1996).
5. W. Yang, M. M. Seidman, W. D. Rupp, Y. Gao, Replisome structure suggests mechanism for continuous fork progression and post-replication repair. *DNA Repair (Amst.)* **81**, 102658 (2019).
6. G. M. Li, The role of mismatch repair in DNA damage-induced apoptosis. *Oncol. Res.* **11**, 393–400 (1999).
7. L. Gu, B. Cline-Brown, F. Zhang, L. Qiu, G. M. Li, Mismatch repair deficiency in hematological malignancies with microsatellite instability. *Oncogene* **21**, 5758–5764 (2002).
8. R. D. Kolodner, G. T. Marsischky, Eukaryotic DNA mismatch repair. *Curr. Opin. Genet. Dev.* **9**, 89–96 (1999).
9. N. Constantin, L. Dzantiev, F. A. Kadyrov, P. Modrich, Human mismatch repair: Reconstitution of a nick-directed bidirectional reaction. *J. Biol. Chem.* **280**, 39752–39761 (2005).
10. Y. Zhang *et al.*, Reconstitution of 5′-directed human mismatch repair in a purified system. *Cell* **122**, 693–705 (2005).
11. L. A. Simmons, B. W. Davies, A. D. Grossman, G. C. Walker, Beta clamp directs localization of mismatch repair in Bacillus subtilis. *Mol. Cell* **29**, 291–301 (2008).
12. H. Hombauer, C. S. Campbell, C. E. Smith, A. Desai, R. D. Kolodner, Visualization of eukaryotic DNA mismatch repair reveals distinct recognition and repair intermediates. *Cell* **147**, 1040–1053 (2011).
13. P. Modrich, DNA mismatch correction. *Annu. Rev. Biochem.* **56**, 435–466 (1987).
14. A. Serra-Cardona, Z. Zhang, Replication-coupled nucleosome assembly in the passage of epigenetic information and cell identity. *Trends Biochem. Sci.* **43**, 136–148 (2018).

15. A. Umar *et al.*, Requirement for PCNA in DNA mismatch repair at a step preceding DNA resynthesis. *Cell* **87**, 65–73 (1996).
16. L. Gu, Y. Hong, S. McCulloch, H. Watanabe, G. M. Li, ATP-dependent interaction of human mismatch repair proteins and dual role of PCNA in mismatch repair. *Nucleic Acids Res.* **26**, 1173–1178 (1998).
17. G. L. Moldovan, B. Pfander, S. Jentsch, PCNA, the maestro of the replication fork. *Cell* **129**, 665–679 (2007).
18. E. M. Boehm, M. S. Gildenberg, M. T. Washington, The many roles of PCNA in eukaryotic DNA replication. *Enzymes* **39**, 231–254 (2016).
19. R. Li, S. Waga, G. J. Hannon, D. Beach, B. Stillman, Differential effects by the p21 CDK inhibitor on PCNA-dependent DNA replication and repair. *Nature* **371**, 534–537 (1994).
20. M. K. Shivji, S. J. Grey, U. P. Strausfeld, R. D. Wood, J. J. Blow, Cip1 inhibits DNA replication but not PCNA-dependent nucleotide excision-repair. *Curr. Biol.* **4**, 1062–1068 (1994).
21. S. J. York, P. Modrich, Mismatch repair-dependent iterative excision at irreparable O6-methylguanine lesions in human nuclear extracts. *J. Biol. Chem.* **281**, 22674–22683 (2006).
22. M. K. Zeman, K. A. Cimprich, Causes and consequences of replication stress. *Nat. Cell Biol.* **16**, 2–9 (2014).
23. D. Gupta, B. Lin, A. Cowan, C. D. Heinen, ATR-Chk1 activation mitigates replication stress caused by mismatch repair-dependent processing of DNA damage. *Proc. Natl. Acad. Sci. U.S.A.* **115**, 1523–1528 (2018).
24. J. Atkinson, P. McGlynn, Replication fork reversal and the maintenance of genome stability. *Nucleic Acids Res.* **37**, 3475–3492 (2009).
25. K. J. Neelsen, M. Lopes, Replication fork reversal in eukaryotes: From dead end to dynamic response. *Nat. Rev. Mol. Cell Biol.* **16**, 207–220 (2015).
26. D. Lemaçon *et al.*, MRE11 and EXO1 nucleases degrade reversed forks and elicit MUS81-dependent fork rescue in BRCA2-deficient cells. *Nat. Commun.* **8**, 860 (2017).
27. F. Ammazzalorso, L. M. Pirzio, M. Bignami, A. Franchitto, P. Pichierri, ATR and ATM differently regulate WRN to prevent DSBs at stalled replication forks and promote replication fork recovery. *EMBO J.* **29**, 3156–3169 (2010).
28. K. Schlacher *et al.*, Double-strand break repair-independent role for BRCA2 in blocking stalled replication fork degradation by MRE11. *Cell* **145**, 529–542 (2011).
29. Y. Wang *et al.*, BASC, a super complex of BRCA1-associated proteins involved in the recognition and repair of aberrant DNA structures. *Genes Dev.* **14**, 927–939 (2000).
30. V. Parkash *et al.*, Structural consequence of the most frequently recurring cancer-associated substitution in DNA polymerase ε. *Nat. Commun.* **10**, 373 (2019).
31. X. Xing *et al.*, A recurrent cancer-associated substitution in DNA polymerase ε produces a hyperactive enzyme. *Nat. Commun.* **10**, 374 (2019).
32. H. D. Li *et al.*, Polymerase-mediated ultramutagenesis in mice produces diverse cancers with high mutational load. *J. Clin. Invest.* **128**, 4179–4191 (2018).
33. H. D. Li *et al.*, A PoleP286R mouse model of endometrial cancer recapitulates high mutational burden and immunotherapy response. *JCI Insight* **5**, e138829 (2020).
34. I. C. Cuevas *et al.*, Fbxw7 is a driver of uterine carcinosarcoma by promoting epithelial-mesenchymal transition. *Proc. Natl. Acad. Sci. U.S.A.* **116**, 25880–25890 (2019).
35. D. Tong *et al.*, Arsenic inhibits DNA mismatch repair by promoting EGFR expression and PCNA phosphorylation. *J. Biol. Chem.* **290**, 14536–14541 (2015).
36. H. G. Gratzner, A. Pollack, D. J. Ingram, R. C. Leif, Deoxyribonucleic acid replication in single cells and chromosomes by immunologic techniques. *J. Histochem. Cytochem.* **24**, 34–39 (1976).
37. G. Saredi *et al.*, H4K20me0 marks post-replicative chromatin and recruits the TONSL–MMS22L DNA repair complex. *Nature* **534**, 714–718 (2016).
38. X. Chen, S. Wei, Y. Ji, X. Guo, F. Yang, Quantitative proteomics using SILAC: Principles, applications, and developments. *Proteomics* **15**, 3175–3192 (2015).
39. H. Dungrawala, D. Cortez, Purification of proteins on newly synthesized DNA using iPOND. *Methods Mol. Biol.* **1228**, 123–131 (2015).
40. A. Quinet, D. Carvajal-Maldonado, D. Lemacon, A. Vindigni, DNA fiber analysis: Mind the gap! *Methods Enzymol.* **591**, 55–82 (2017).
41. R. Zellweger *et al.*, Rad51-mediated replication fork reversal is a global response to genotoxic treatments in human cells. *J. Cell Biol.* **208**, 563–579 (2015).
42. K. Rickman, A. Smogorzewska, Advances in understanding DNA processing and protection at stalled replication forks. *J. Cell Biol.* **218**, 1096–1107 (2019).
43. A. T. Vo *et al.*, hMRE11 deficiency leads to microsatellite instability and defective DNA mismatch repair. *EMBO Rep.* **6**, 438–444 (2005).
44. L. Maresca *et al.*, Functional interaction between *BRCA1* and DNA repair in yeast may uncover a role of *RAD50, RAD51, MRE11A*, and *MSH6* somatic variants in cancer development. *Front. Genet.* **9**, 397 (2018).
45. X. Lyu *et al.*, Human CST complex protects stalled replication forks by directly blocking MRE11 degradation of nascent-strand DNA. *EMBO J.* **40**, e103654 (2021).
46. K. Schlacher *et al.*, "Double-strand break repair-independent role for BRCA2 in blocking stalled replication fork degradation by MRE11" in *Cell* (Cell Press, 2011), pp. 529–542.
47. S. Thangavel *et al.*, DNA2 drives processing and restart of reversed replication forks in human cells. *J. Cell Biol.* **208**, 545–562 (2015).
48. J. J. Kim *et al.*, PCAF-mediated histone acetylation promotes replication fork degradation by MRE11 and EXO1 in BRCA-deficient cells. *Mol. Cell* **80**, 327–344.e8 (2020).
49. D. Branzei, M. Foiani, Maintaining genome stability at the replication fork. *Nat. Rev. Mol. Cell Biol.* **11**, 208–219 (2010).
50. W. Feng, S. C. Di Rienzi, M. K. Raghuraman, B. J. Brewer, Replication stress-induced chromosome breakage is correlated with replication fork progression and is preceded by single-stranded DNA formation. *G3 (Bethesda)* **1**, 327–335 (2011).
51. V. Naim, F. Rosselli, The FANC pathway and mitosis: A replication legacy. *Cell Cycle* **8**, 2907–2911 (2009).
52. R. Fishel, Signaling mismatch repair in cancer. *Nat. Med.* **5**, 1239–1241 (1999).
53. J. Ortega, G. S. Lee, L. Gu, W. Yang, G. M. Li, Mispair-bound human MutS-MutL complex triggers DNA incisions and activates mismatch repair. *Cell Res.* **31**, 542–553 (2021).
54. H. Liao, F. Ji, T. Helleday, S. Ying, Mechanisms for stalled replication fork stabilization: New targets for synthetic lethality strategies in cancer treatments. *EMBO Rep.* **19**, e46263 (2018).
55. J. Guan *et al.*, MLH1 deficiency-triggered DNA hyperexcision by Exonuclease 1 activates the cGAS-STING pathway. *Cancer Cell* **39**, 109–121.e5 (2021).
56. C. Lu *et al.*, DNA sensing in mismatch repair-deficient tumor cells is essential for anti-tumor immunity. *Cancer Cell* **39**, 96–108.e6 (2021).
57. G. M. Li, P. Modrich, Restoration of mismatch repair to nuclear extracts of H6 colorectal tumor cells by a heterodimer of human MutL homologs. *Proc. Natl. Acad. Sci. U.S.A.* **92**, 1950–1954 (1995).
58. A. Emam *et al.*, Stalled replication fork protection limits cGAS-STING and P-body-dependent innate immune signalling. *Nat. Cell Biol.* **24**, 1154–1164 (2022).
59. F. Li *et al.*, The histone mark H3K36me3 regulates human DNA mismatch repair through its interaction with MutSα. *Cell* **153**, 590–600 (2013).